Title

Deep Convolutional Neural Network for Dedicated Regions-of-Interest Based Multi-Parameter Quantitative Ultrashort Echo Time (UTE) Magnetic Resonance Imaging of the Knee Joint

Journal

Journal of Imaging Informatics in Medicine, 37(5)

ISSN

2948-2925

Authors

Lu, Xing

Ma, Yajun

Chang, Eric Y

et al.

Publication Date

2024-10-01

DOI

10.1007/s10278-024-01089-8

Peer reviewed

Journal of Imaging Informatics in Medicine (2024) 37:2126–2134
https://doi.org/10.1007/s10278-024-01089-8

Deep Convolutional Neural Network for Dedicated Regions-of-Interest Based Multi-Parameter Quantitative Ultrashort Echo Time (UTE) Magnetic Resonance Imaging of the Knee Joint

Xing Lu[1] · Yajun Ma[1] · Eric Y. Chang[1,2] · Jiyo Athertya[1] · Hyungseok Jang[1] · Saeed Jerban[1] · Dana C. Covey[3] · Susan Bukata[3] · Christine B. Chung[1,2] · Jiang Du[1,2,4]

Received: 4 September 2023 / Revised: 10 March 2024 / Accepted: 11 March 2024 / Published online: 28 March 2024

Abstract

We proposed an end-to-end deep learning convolutional neural network (DCNN) for region-of-interest based multi-parameter quantification (RMQ-Net) to accelerate quantitative ultrashort echo time (UTE) MRI of the knee joint with automatic multi-tissue segmentation and relaxometry mapping. The study involved UTE-based T1 (UTE-T1) and Adiabatic T1ρ (UTE-AdiabT1ρ) mapping of the knee joint of 65 human subjects, including 20 normal controls, 29 with doubtful-minimal osteoarthritis (OA), and 16 with moderate-severe OA. Comparison studies were performed on UTE-T1 and UTE-AdiabT1ρ measurements using 100%, 43%, 26%, and 18% UTE MRI data as the inputs and the effects on the prediction quality of the RMQ-Net. The RMQ-net was modified and retrained accordingly with different combinations of inputs. Both ROI-based and voxel-based Pearson correlation analyses were performed. High Pearson correlation coefficients were achieved between the RMQ-Net predicted UTE-T1 and UTE-AdiabT1ρ results and the ground truth for segmented cartilage with acceleration factors ranging from 2.3 to 5.7. With an acceleration factor of 5.7, the Pearson *r*-value achieved 0.908 (ROI-based) and 0.945 (voxel-based) for UTE-T1, and 0.733 (ROI-based) and 0.895 (voxel-based) for UTE-AdiabT1ρ, correspondingly. The results demonstrated that RMQ-net can significantly accelerate quantitative UTE imaging with automated segmentation of articular cartilage in the knee joint.

Keywords Quantitative MRI · Automated segmentation · DCNN · RMQ-Net · UTE · Knee joint · OA

Introduction

Osteoarthritis (OA) is generally considered a heterogeneous and multifactorial disease associated with progressive loss of articular cartilage [1]. Recent understanding of OA has shifted from a cartilage-centric focus to the concept of "whole organ disease" [2]. Human knee joints are composed of different tissues that interact and allow joints to function over long periods of time. When one joint tissue begins to deteriorate, it will likely affect other joint tissues and ultimately contribute to the failure of the joint as a whole [3]. Unfortunately, conventional magnetic resonance imaging (MRI) sequences can only assess long T_2 tissues or tissue components, such as the more superficial layers of articular cartilage, synovium, muscle, and fat. Many knee joint tissues or tissue components, such as the deep cartilage and osteochondral junction, menisci, ligaments, tendons, and bone, have short T_2s and show little signal with clinical sequences [4–6]. Ultrashort echo time (UTE) sequences with echo times (TEs) of less than 0.1 ms allow direct morphological imaging of both short and long T_2 tissues in the knee joint [6–8]. A series of quantitative UTE MRI techniques, including T1 [9, 10], T1ρ [11, 12], Adiabatic T1ρ (AdiabT1ρ) [13], T2* [14, 15], magnetization transfer [16], perfusion [17], diffusion [18, 19], and quantitative susceptibility mapping [20, 21],

✉ Jiang Du
jiangdu@health.ucsd.edu

1 Department of Radiology, University of California, 9452 Medical Center Dr, San Diego, San Diego, CA 92037, USA

2 Radiology Service, Veterans Affairs San Diego Healthcare System, San Diego, CA, USA

3 Department of Orthopaedic Surgery, University of California, San Diego, CA, USA

4 Department of Bioengineering, University of California, San Diego, CA, USA

have also been developed to probe biochemical alterations in all major knee joint tissues, thereby providing a truly "whole organ disease" approach for more comprehensive assessment of OA.

Compared with qualitative MRI, quantitative MRI (qMRI) is a more accurate approach to evaluating underlying pathology and disease course [22]. However, qMRI is typically much more time-consuming due to the requirement of repeated data acquisitions, for example, different repetition times (TRs) or flip angles (FAs) for T1 mapping [9, 10], different spin-locking times (TSLs) for T1ρ or AdiabT1ρ mapping [11–13], and different echo times (TEs) for T2* mapping [14, 15]. Another challenge is related to the various knee joint tissues involved in OA, which can now be evaluated with UTE sequences. Conventional MRI cannot quantify short T2 tissues and focuses mainly on the superficial layers of articular cartilage. On the other hand, UTE MRI allows quantifying both short and long T2 tissues in the knee joint. Segmenting and quantitatively mapping the various knee joint tissues are much more complicated and time-consuming.

Deep convolutional neural networks (DCNN) are feasible methods for accurately segmenting multi-component organs in medical imaging analysis [23, 24]. There has recently been intense interest in employing DCNN models to obtain faster quantitative mapping of MRI parameters, with or without physics information [25–27]. Deep learning models with multi-task or multi-head design, generally with one as the major task and others as auxiliary tasks with weaker constraints, have been widely used in deep learning architectures to finish several tasks simultaneously. Multitasking is important for handling complex tasks simultaneously and has been widely used in medical imaging. Normally, the architecture for the multitask design could be categorized into cascaded, parallel, interacted, and hybrid [28]. In medical imaging, the multitask design is normally used for simultaneous segmentation and classification or regression of the lesion [29–31]. The reconstruction and segmentation can also be simultaneously performed [32, 33]. Also, the limitations on the auxiliary task constraint normally would help improve the performance of the major task. The multi-task design strategy can be used to segment and quantify knee joint tissues.

In this study, a region-of-interest based multiple parameters quantitative MRI network (RMQ-net) was introduced to accelerate UTE-based qMRI while providing automatic tissue segmentation and relaxometry mapping based on a parallel multitask design. The efficacy of the RMQ-net was demonstrated on UTE-based T1 (UTE-T1) and AdiabT1ρ (UTE-AdiabT1ρ) mapping of articular cartilage in the knee joint [9–13].

Method

Subjects

The study was approved by the local Institutional Review Board. A total of 65 human subjects (54.8 ± 16.9 years; 33 females) were included in the study. The whole knee joint (29 left, 36 right) was scanned using a transmit/receive 8-channel knee coil on a 3-T clinical MR system (MR750, GE Healthcare Technologies, Inc.). Informed consent was obtained from each subject. According to the condensed Kellgren–Lawrence (KL) grade [34], subjects were categorized into three groups: normal controls ($n = 20$, KL = 0), doubtful-minimal OA ($n = 29$, KL = 1–2), and moderate-severe OA ($n = 16$, KL = 3–4).

Data Acquisition, Preparation, and Pre-processing

Three-dimensional UTE cones data sampling was performed using a TE of 32 μs, a TR of 20 ms, and FAs of 5°, 10°, 20°, and 30°, respectively, with a scan time of 2 min 22 s for each flip angle for UTE-T1 mapping [10]. Multiple spokes (N_{sp}) were acquired after each Adiab$T_{1\rho}$ preparation to speed up data acquisition. For UTE-AdiabT1ρ mapping, the scan parameters included a TR of 500 ms, an FA of 10°, an Nsp of 25, and 7 TSLs of 0, 12, 24, 36, 48, 72, and 96 ms, with a scan time of 2 min 34 s for each TSL [13]. Other imaging parameters included a field of view (FOV) of 15 × 15 × 10.8 cm^3, a data acquisition matrix size of 256 × 256 × 36, a slice thickness of 3.0 mm, an acquired voxel size of 0.59 × 0.59 × 3.0 mm^3, and a sampling bandwidth of 166 kHz. Additionally, B1 mapping was achieved using 3D UTE cones actual flip angle imaging (AFI) with two interleaved TRs of 20 and 100 ms, an FA of 45°, a reduced matrix size of 128 × 128 × 18, and a total scan time of 4 min 57 s [9].

The UTE raw data were acquired in k-space following the 3D Cones trajectories. These complex-valued data were regridded onto a 3D Cartesian space, followed by fast Fourier transform to generate complex image data. Magnitude images were then generated. Subsequently, motion registration was applied to all 3D UTE magnitude images using the Elastix software, where a rigid affine transform was followed by a non-rigid b-spline registration [35, 36]. Multiple parametric maps from all acquired data were taken as ground truth (GT) and obtained using MATLAB 2017b (The MathWorks, Inc.). M0, UTE-T1, UTE-AdiabT1ρ, and B1 maps were obtained via non-linear fitting using the Levenberg-Marquardt algorithm [10, 13]. The fatty areas, such as the bone marrow regions, which had low signal intensity due to fat suppression in

UTE-AdiabT1ρ imaging, were removed in the ground truth map through simple thresholding. Regions of interest (ROIs) for the cartilage area were labeled with homemade Matlab code by one experienced radiologist with over 15 years of experience in musculoskeletal radiology. Real values were used as the input MRI signals for the RMQ-Net.

A total of 1200 slice images from 50 subjects (including healthy volunteers and patients with different degrees of OA) were used for model training, and 366 images of 15 additional subjects were used for model validation. The data split was accomplished at the patient level. All slices from the same subject were assigned to the training, testing, or validation cohort. The DCNNs were designed and trained with PyTorch 1.1.0 on a workstation with an Nvidia GTX 1080 Ti (11 GB GPU memory).

Network Design

The RMQ-Net was designed based on a U-Net style DCNN but with two branches for outputs, named Reg_branch and Seg_branch (Fig. 1). The input of the RMQ-net is MRI signals with different FAs and TSLs. The input channel number of the first layer in the network was modified according to the input MRI signals. Along the encoder path, down-samplings were applied to enable subsequent feature extractions. Latent features were shared for up-sampling operations of both branches. Between convolutional blocks, skip connections were established. For the Reg_branch, quantitative MRI parameter maps (M0, T1, B1, and T1ρ) were generated according to the voxel-fitting-based maps as the ground truth, with L1 loss (loss_{map}) as the constraint, as shown in Eq. (1).

$$loss_{map} = l1\left(Y, \hat{Y}\right) Y = [M0, T1, B1, T1\rho] \tag{1}$$

where Y is the ground truth mapping generated by conventional fitting procedure and $\hat{Y}$ is the prediction maps for M0, T1, B1, and T1ρ. For each parametric map, a dedicated Reg_branch is needed.

For Seg_branch, the cartilage mask was generated using segmentation loss (loss_{seg}), which is based on the binary cross entropy loss ($loss_{bce}$) and dice loss ($loss_{dice}$), as shown in Eq. (2).

$$loss_{seg} = \lambda loss_{bce} + (1 - \lambda) loss_{dice} \tag{2}$$

where λ is the weight for binary cross entropy loss. The total loss for RMQ-Net ($\text{loss}_{\text{total}}$) consists of loss_{map} and loss_{seg}, as shown in Eq. (3).

$$loss_{total} = \gamma_1 loss_{map} + \gamma_2 loss_{seg} \tag{3}$$

To evaluate the efficacy of accelerated quantitative UTE MRI, inputs of the VMQ-net consist of a series of combinations of UTE MRI data with different FAs and TSLs. In total, five different combinations were investigated, including four FAs and seven TSLs (4FAs + 7TSLs) (total scan time of 32 min 38 s), two FAs and three TSLs (2FAs + 3TSLs) (total scan time of 14 min 2 s), one FA and two TSLs (1FAs + 2TSLs) (total scan time of 8 min 18 s), and one FA and one TSL (5 min 44 s). Details of the selected FAs and TSLs can be found in Table 1. The outputs of the RMQ-Net include multi-parameter mapping (UTE-T1 and UTE-AdiabT1ρ) and multi-ROIs (e.g., cartilage, menisci, ligaments, and tendons). The multi-parameter maps and segmented ROIs can be directly multiplied to generate perspective

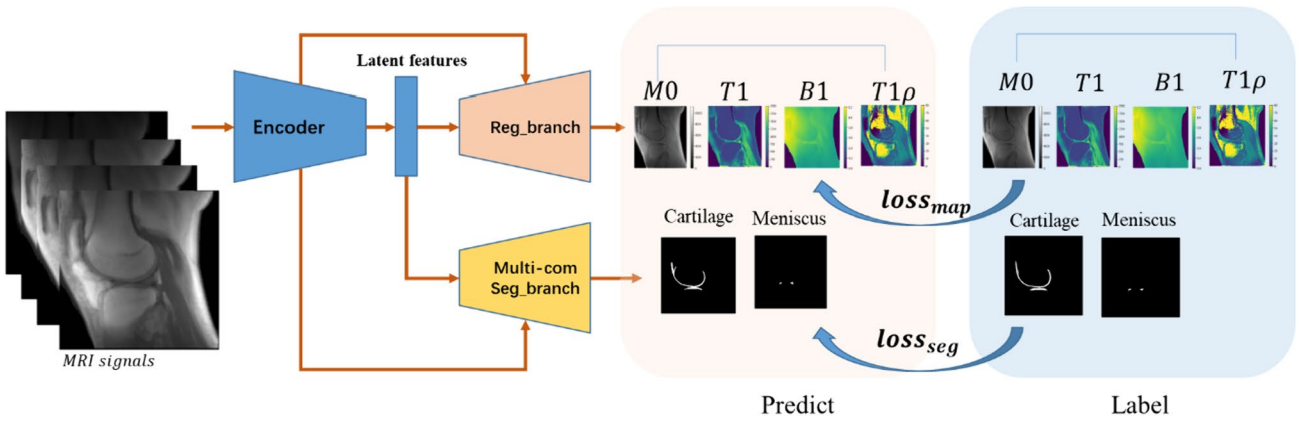

Fig. 1 Network architecture for the proposed RMQ-Net was designed based on a 5-layer modified Unet architecture with two branches. The Reg_branch generates quantitative MRI mapping (M0, T1, B1, and T1ρ). The Seg_branch generates the segmentation of various knee joint tissue components, such as cartilage, meniscus, and ligaments (focusing on the articular cartilage in this study)

quantitative relaxometry maps for each knee joint tissue. For simplicity, only the articular cartilage was investigated in this feasibility study.

Training and Testing

The design and implementation of RMQ-Net were based on PyTorch 1.1.0 using a workstation with an Nvidia GTX 1080 Ti (11 GB GPU memory). Hyper-parameters for training the RMQ-net included the optimizer of Adam, a learning rate from 0.001 with a 3-steps cosine-annealing strategy, and epochs of 600. Models of different inputs combined with the lowest $loss_{total}$ during training were saved as the best model for further evaluation.

Evaluation

Pearson correlation analyses were carried out to evaluate the performance and efficiency of RMQ-net with different combinations of UTE MRI data input as outlined in Table 1. Automatic segmentation based on the RMQ-net generated masks for the articular cartilage and menisci, which were compared with the manual segmentation by the experienced radiologist (the ground truth) using Pearson correlation analyses. Both ROI-based (mean UTE-T1 and UTE-AdiabT1ρ values for cartilage in each slice) and voxel-based (UTE-T1 and UTE-AdiabT1ρ values for each voxel in the segmented cartilage regions) analyses were performed. Normalized L2 (normalized root mean squared error) and L1 (normalized mean or median absolute difference) metrics were also calculated. The statistics were analyzed with Python scipy packages [37] .

Results

Accelerated Quantitative UTE MRI with the RMQ-net

Four different combinations of UTE MRI data were assembled as inputs of the RMQ-net to test the feasibility of accelerated quantification, as shown in Table 1. Representative ground truth and predicated T1_map and T1ρ_map results for the articular cartilage with different combinations of inputs, including 1FA + 2TSLs, 2FAs + 3TSLs, and 4FAs + 7TSLs, are shown in Fig. 2.

Correlations Between RMQ-net Segmented Quantitative Results and the Ground Truth

For the RMQ-net segmented cartilage, Pearson correlations between the ROI-based ground truth and predicted UTE-T1 results can be found in Fig. 3, where *r*-values slightly decreased with fewer FAs and TSLs. The correlation *r*-values are 0.918 for 4FAs + 7TSLs, 0.911 for 2FAs + 3TSLs, 0.904 for 1FA + 2TSLs, and 0.907 for 1FA + 1TSL. The *r*-value remains largely unchanged while the total scan time is reduced by up to 5.7-fold, suggesting that the cartilage area can be robustly segmented and quantified with a fraction of the total qMRI data.

Figure 4 shows the Pearson correlations between the voxel-based ground truth and predicted UTE-T1 results, where *r*-values slightly decreased from 0.985 for 4FAs + 7TSLs, to 0.965 for 2FAs + 3TSLs, 0.963 for 1FA + 2TSLs, and 0.945 for 1FA + 1TSL. The high *r*-values further demonstrate the efficacy of the RMQ-net for automatic segmentation and accelerated quantitative UTE-T1 mapping of articular cartilage.

Table 1 The estimated scan time, acceleration factor, flip angles, spin-locking times, and the corresponding Pearson correlation coefficients and *P* values between the ROI-based and voxel-based ground truth and the RMQ-Net predicted UTE-T1 and UTE-AdiabT1ρ results for four different combinations of 4FAs + 7TSLs, 2FAs + 3TSLs, 1FA + 2TSLs, and 1FA + 1TSL

Inputs	Estimated scan time (minutes)	Acceleration factor	FAs (degree)	TSLs (ms)	Pearson correlation between predicted and ground truth ROI (*p* values)		Pearson correlation between predicted and ground truth of voxel (*p* values)	
					T1_cartilage	T1ρ_cartilage	T1_cartilage	T1ρ_cartilage
4FAs + 7TSLs	32.63	1	5, 10, 20, 30	0, 12, 24, 36, 48, 72, 96	0.918 ($p < 0.0001$)	0.816 ($p < 0.0001$)	0.985 ($p < 0.0001$)	0.969 ($p < 0.0001$)
2FAs + 3TSLs	14.03	2.3	5,30	12, 36, 72	0.912 ($p < 0.0001$)	0.841 ($p < 0.0001$)	0.965 ($p < 0.0001$)	0.910 ($p < 0.0001$)
1FA + 2TSLs	8.3	3.9	30	12, 72	0.904 ($p < 0.0001$)	0.785 ($p < 0.0001$)	0.963 ($p < 0.0001$)	0.914 ($p < 0.0001$)
1FA + 1TSL	5.73	5.7	20	48	0.908 ($p < 0.0001$)	0.733 ($p < 0.0001$)	0.945 ($p < 0.0001$)	0.895 ($p < 0.0001$)

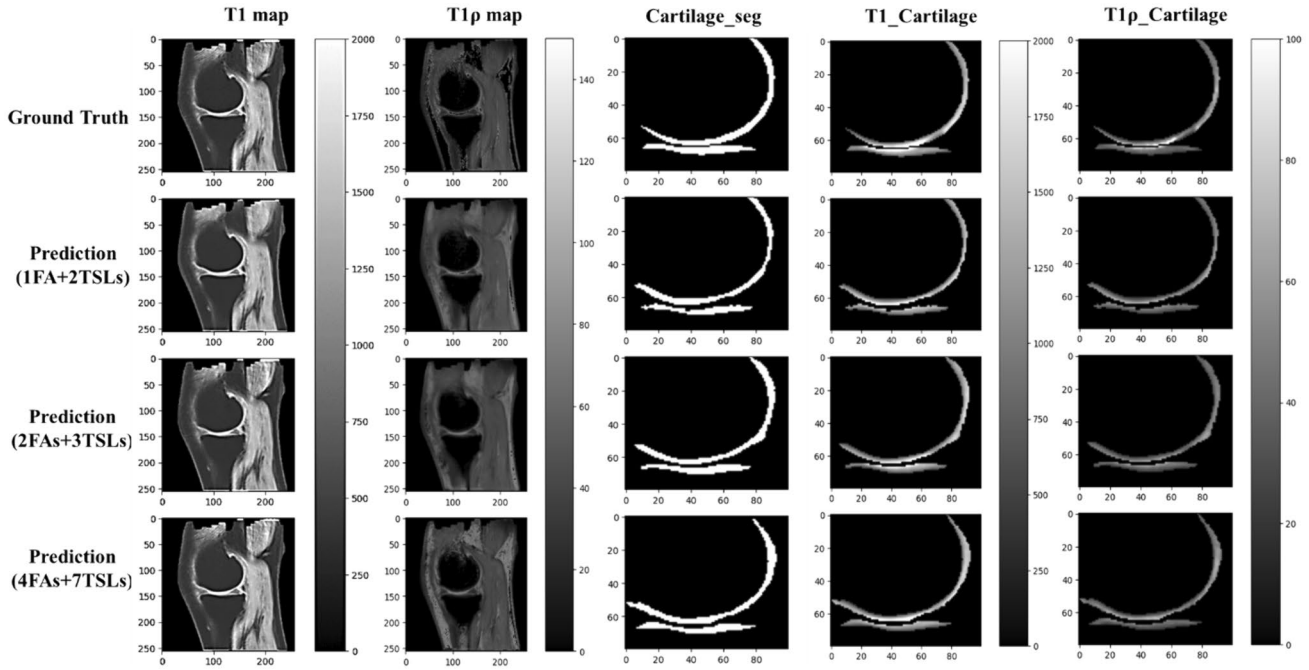

Fig. 2 Representative ground truth (1st row) and predicted UTE-T1 (1st column) and UTE-T1ρ (2nd column) mapping based on 1FA + 2TSLs (2nd row), 2FAs + 3TSLs (3rd row), and 4FAs + 7TSLs (4th row), as well as the automated segmentation of the femoral and tibial articular cartilage (Cartilage_Seg, 3rd column), and the corresponding T1 (T1_Cartilage, 4th column) and T1ρ maps (T1ρ_Cartilage, 5th column)

Figure 5 shows the correlation study between the RMQ-net generated UTE-AdiabT1ρ values from automatically segmented cartilage and the ground truth from an experienced MSK radiologist. The *r*-values vary from 0.816 for 4FAs + 7TSLs, to 0.841 for 2FAs + 3TSLs, 0.785 for 1FA + 2TSLs, and 0.733 for 1FA + 1TSLs. Improved Pearson correlations were observed between the voxel-based

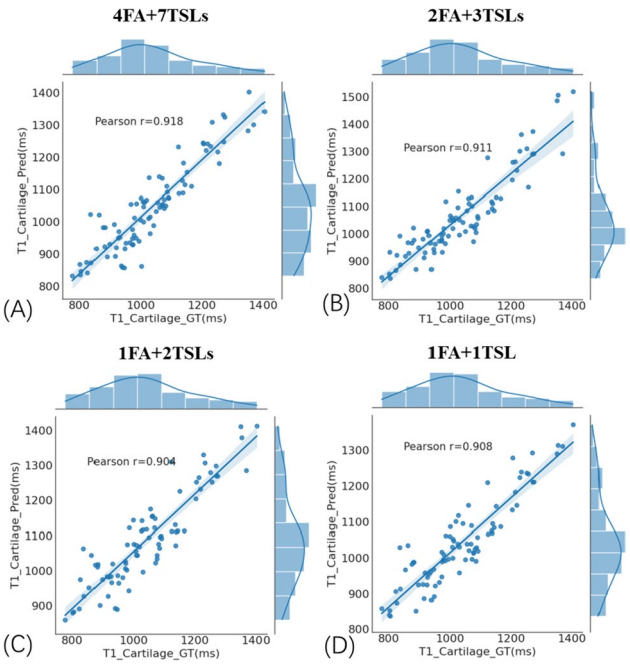

Fig. 3 ROI-based correlation between the ground truth cartilage T1 (T1_Cartilage_GT) and the RMQ-Net predicted cartilage T1 (T1_Cartilage_pred) results for 4FAs + 7TSLs (**A**), 2FAs + 3TSLs (**B**), 1FA + 2TSLs (**C**), and 1FA + 1TSL (**D**), with Pearson correlations of 0.918, 0.911, 0.904, and 0.908, respectively

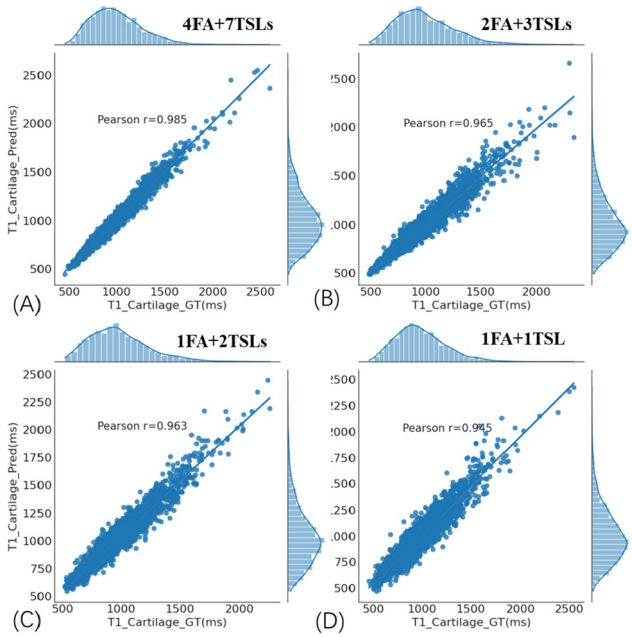

Fig. 4 Voxel-based correlation between the ground truth cartilage T1 and the RMQ-Net predicted cartilage T1 results for 4FAs + 7TSLs (**A**), 2FAs + 3TSLs (**B**), 1FA + 2TSLs (**C**), and 1FA + 1TSL (**D**), with Pearson correlations of 0.985, 0.965, 0.963, and 0.945, respectively

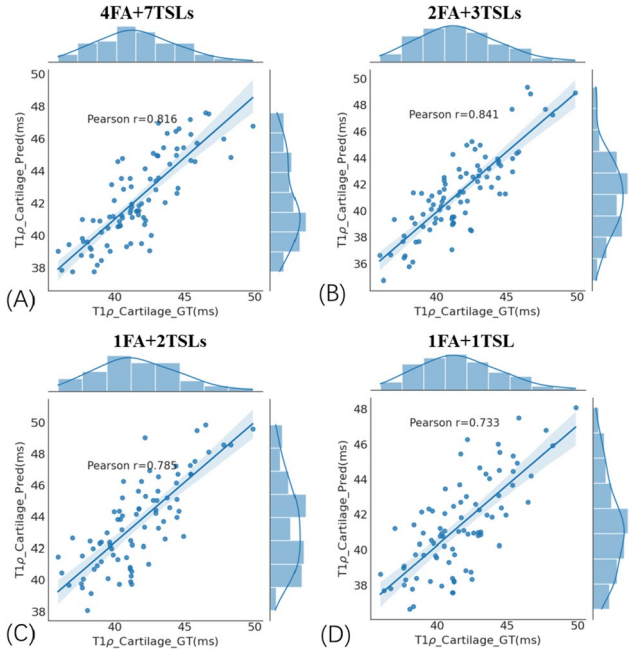

Fig. 5 ROI-based correlation between the ground truth and the RMQ-Net predicted UTE-AdiabT1ρ results for four combinations of 4FAs + 7TSLs (**A**), 2FAs + 3TSLs (**B**), 1FA + 2TSLs (**C**), and 1FA + 1TSL (**D**), with Pearson correlations of 0.816, 0.841, 0.785, and 0.733, respectively

ground truth and predicted UTE-T1ρ results (Fig. 6), where *r*-values varied from 0.969 for 4FAs + 7TSLs, to 0.910 for 2FAs + 3TSLs, 0.914 for 1FA + 2TSLs, and 0.895 for

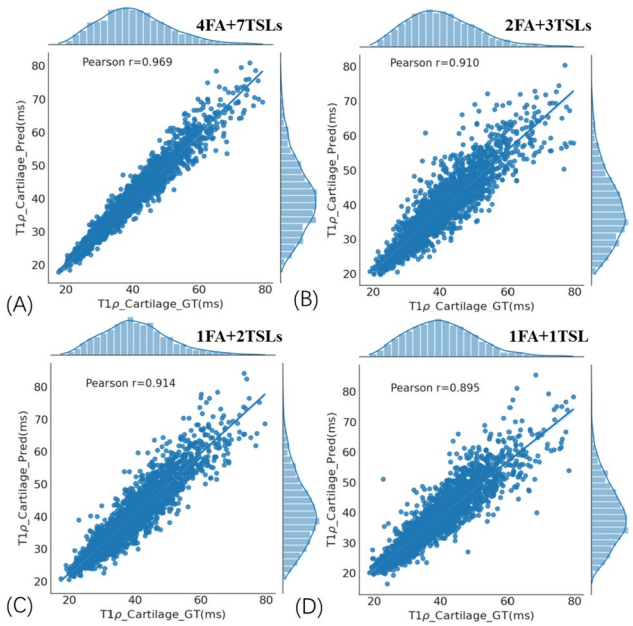

Fig. 6 Voxel-based correlation between the ground truth cartilage T1ρ and the RMQ-Net predicted cartilage T1ρ results for 4FAs + 7TSLs (**A**), 2FAs + 3TSLs (**B**), 1FA + 2TSLs (**C**), and 1FA + 1TSL (**D**), with Pearson correlations of 0.969, 0.910, 0.914, and 0.895, respectively

Table 2 Normalized L1 and L2 errors between the ground truth and the RMQ-Net predicted UTE-T1 and UTE-AdiabT1ρ results for four different combinations of 4FAs + 7TSLs, 2FAs + 3TSLs, 1FA + 2TSLs, and 1FA + 1TSL

Inputs	L1 error (mean ± std)		L2 error (mean ± std)		Normalized L1 error (mean ± std)		Normalized L2 error (mean ± std)	
	T1	T1ρ	T1	T1ρ	T1(%)	T1ρ (%)	T1(%)	T1ρ (%)
4FAs + 7TSLs	36.03 ± 13.54	1.96 ± 0.42	1.86 ± 0.74	0.11 ± 0.05	3.62 ± 1.2	4.89 ± 1.06	0.19 ± 0.7	0.28 ± 0.15
2FAs + 3TSLs	53.37 ± 17.81	3.55 ± 1.01	2.96 ± 1.19	0.21 ± 0.11	5.36 ± 1.52	8.72 ± 2.33	0.30 ± 0.12	0.49 ± 0.26
1FA + 2TSLs	67.88 ± 19.12	3.48 ± 1.01	3.63 ± 1.43	0.21 ± 0.12	6.94 ± 2.02	8.61 ± 2.39	0.37 ± 0.16	0.49 ± 0.27
1FA + 1TSL	67.07 ± 18.12	3.69 ± 1.1	3.84 ± 2.28	0.22 ± 0.15	6.83 ± 1.74	9.06 ± 2.38	0.39 ± 0.23	0.54 ± 0.35

1FA + 1TSL. These results also suggest that the RMQ-net can automatically segment articular cartilage and accelerate quantitative UTE-T1ρ mapping.

Table 1 summarizes the four UTE MRI input data combinations and the corresponding Pearson correlation coefficients between the ROI-based and voxel-based ground truth and the RMQ-Net predicted UTE-T1 and UTE-AdiabT1ρ results. Normalized L1 and L2 errors are listed in Table 2. These results confirm the efficacy of the RMQ-net for simultaneous segmentation and multi-parameter quantitative mapping of articular cartilage in the knee joint.

Discussion

Quantitative MRI analysis based on ROIs has received increasing attention in clinical settings, as it can better investigate the pathogenesis and diagnostic basis of various diseases [38, 39] . However, the relatively long data acquisition time and associated time-consuming manual operations (e.g., segmentation and curve fitting) are major obstacles. In this study, we proposed a multi-parameter quantitative MRI method based on ROIs using DCNNs. The RMQ-net allows simultaneous segmentation of knee joint tissues and quantitative UTE-T1 and UTE-AdiabT1ρ mapping with reduced MRI data inputs. High Pearson correlation coefficients were achieved between the ground truth and the RMQ-Net predicted UTE-T1 and UTE-AdiabT1ρ results for all acceleration factors ranging from 2.3 to 5.7. A 5.7-fold acceleration leads to only 4% decrease in the Pearson correlation for UTE-T1. UTE-AdiabT1ρ is subject to more significant error, with 10% decrease in the Pearson correlation for an acceleration factor of 5.7. This correlation is reduced by 6% for an acceleration factor of 3.9 and 4% for an acceleration factor of 2.3. These results suggest that the RMQ-net allows for accurate simultaneous segmentation and multi-parameter quantitative mapping of articular cartilage in the knee joint. The accelerated automated UTE qMRI likely benefits future clinical translational studies in OA.

The feasibility of simultaneous segmentation and quantification based on DCNNs has been further validated in this study, which is the base for the ROIs-based quantitative analysis. The framework of the DCNNs used in this study is the encoder-decoder structure with multi-task design, with the generation of qMRI mapping as the major task and the ROIs segmentation as the auxiliary task. Multi-task design is not rare in the medical image domain, such as the classification with segmentation [40, 41] , or classification with image generation [42] , where classification always be used as an auxiliary task for the segmentation and the image generation is used as an auxiliary task for the classification. However, the combination of image generation, physical quantification, and segmentation as an auxiliary task has still not been fully studied. In this study, UTE-based MRI parametric mapping could be taken as an image generation task with physical information constraints. It has been initially tested that the physics information can be useful for improving quantification accuracy by adding the physics loss design. However, it still needs further exploration of how much it could affect the results with different weights of the loss. Also, in further study, generative adversarial network (GAN)-based image generation might be more promising for the generated quantitative mapping details with physics information considered in the loss design [43] .

The major benefit of the RMQ-net is that it may dramatically reduce the MRI scan time. In this feasibility study, we found that reasonable quantitative maps and segmentation predictions could be generated with much reduced input of UTE MRI data. With reduced FAs and TSLs, it could be observed that the ROIs-based *r*-values decrease slightly while the total scan time is reduced by fourfold. Therefore, it is an efficient technique for accelerated qMRI without compromising quantitative accuracy. For further studies, we will continue optimizing the network structure by introducing transformer and diffusion modules to stabilize the output prediction of both the quantification mapping and the segmentations. We will also explore reducing the sampling points of the MRI scan sequences, which may further reduce the total scan time for clinical applications.

There are several limitations to this study. Firstly, the backbone for this study is based on a simple Unet, which has the potential for further improvement of the performance with transformer and diffusion models. Secondly, only UTE MRI images were used for this study, as they may not lose generality, and more MRI images may be needed for further validation. Thirdly, only 2D images were studied in this paper. It will be tested on the 3D volume and quantification in further study. Fourthly, the cartilage region was annotated by only one radiologist, who might introduce some annotation bias. Fifthly, TSL and FA are empirically chosen for magnitude processing. Further optimization of spin-lock times and curve fitting based on complex-valued data may improve UTE-T1 and UTE-AdiabT1ρ mapping [44].

Conclusion

This study proposes an end-to-end deep learning neural network framework to simultaneously obtain multiple parameters qMRI map and the ROIs quickly and accurately. Testing it on UTE-T1 and UTE-AdiabT1ρ mapping demonstrated that the RMQ-net could get reasonable results for both qMRI mapping and regional value analysis. More

ROI regions and qMRI maps could easily be extended for simultaneous generation based on this RMQ-net framework in the future.

Funding The authors acknowledge grant support from the National Institutes of Health (RF1AG075717, R01AR062581, R01AR068987, R01AR075825, R01AR079484, P30AR073761, and R21AR075851), the VA Clinical Science Research & Development Service (I01CX002211, I01CX001388, and 1I01BX005952), and GE Healthcare.

References

1. Buckwalter JA, Martin J. Degenerative joint disease. Clin Symp 1995; 47:1-32.
2. Hayashi D, Guermazi A, Hunter DJ. OARSI year in review 2010: imaging. Osteoarthritis Cartilage 2011; 19:354-360.
3. Brandt KD, Radin EL, Dieppe PA, Putte L. Yet more evidence that osteoarthritis is not a cartilage disease (Editorial). Ann Rheum Dis 2006; 65:1261-1264.
4. Gatehouse PD, Bydder GM. Magnetic resonance imaging of short T2 components in tissue. Clin Radiol 2003; 58:1-19.
5. Ma Y, Jang H, Jerban S, et al. Making the invisible visible-ultrashort echo time magnetic resonance imaging: technical developments and applications. Appl Phys Rev. 2022;9(4):041303.
6. Gold GE, Thedens DR, Pauly JM, Fechner KP, Bergman G, Beaulieu CF, Macovski A. MR imaging of articular cartilage of the knee: new methods using ultrashort TEs. AJR Am J Roentgenol 1998; 170:1223-1226.
7. Chang EY, Du J, Chung CB. UTE imaging in the musculoskeletal system. J Magn Reson Imaging 2015; 41(4):870-883.
8. Afsahi AM, Ma Y, Jang H, et al. Ultrashort echo time magnetic resonance imaging techniques: met and unmet needs in musculoskeletal imaging. J Magn Reson Imaging 2022; 55(6):1597-612.
9. Ma YJ, Lu X, Carl M, Zhu Y, Szeverenyi N, Bydder GM, Chang E, Du J. Accurate T1 mapping of short T2 tissues using a three-dimensional ultrashort echo time cones actual flip angle – variable TR (3D UTE-Cones AFI-VTR) method. Magn Reson Med 2018; 80:598-608.
10. Ma YJ, Zhao W, Wan L, Guo T, Searleman A, Jang H, Chang EY, Du J. Whole knee joint T1 values measured in vivo at 3T by combined 3D ultrashort echo time cones actual flip angle and variable flip angle methods. Magn Reson Med 2019; 81:1634-1644.
11. Du J, Carl M, Diaz E, et al. Ultrashort TE T1rho (UTE T1rho) imaging of the Achilles tendon and meniscus. Magn Reson Med 2010; 64:834-842.
12. Ma YJ, Carl M, Shao H, Tadros AS, Chang EY, Du J. Three-dimensional ultrashort echo time cones T1rho (3D UTE-cones-T1rho) imaging. NMR Biomed 2017; 30:e3709.
13. Ma Y, Carl M, Searleman A, Lu X, Chang EY, Du J. Three dimensional adiabatic T1ρ prepared ultrashort echo time Cones (3D AdiabT1ρ UTE-Cones) sequence for whole knee imaging. Magn Reson Med 2018; 80:1429-1439.
14. Williams A, Qian Y, Bear D, Chu CR. Assessing degeneration of human articular cartilage with ultra-short echo time (UTE) T2* mapping. Osteoarthritis Cartilage 2010; 18(4):539-46.
15. Chu CR, Williams AA, West RV, et al. Quantitative magnetic resonance imaging UTE-T2* mapping of cartilage and meniscus healing after anatomic anterior cruciate ligament reconstruction. Am J Sports Med 2014; 42(8):1847-56.
16. Ma YJ, Chang EY, Carl M, Du J. Quantitative magnetization transfer ultrashort echo time imaging using a time-efficient 3D multispoke Cones sequence. Magn Reson Med 2018; 79(2):692-700.
17. Wan L, Wu M, Sheth V, et al. Evaluation of cortical bone perfusion using dynamic contrast enhanced ultrashort echo time imaging: a feasibility study. Quant Imaging Med Surg 2019; 9(8):1383-1393.
18. Chaudhari AS, Sveinsson B, Moran CJ, et al. Imaging and T2 relaxometry of short-T2 connective tissues in the knee using ultrashort echo-time double-echo steady-state (UTEDESS). Magn Reson Med 2017; 78(6):2136-2148.
19. Jang H, Ma Y, Carl M, Jerban S, Chang EY, Du J. Ultrashort echo time Cones double echo steady state (UTE-Cones-DESS) for rapid morphological imaging of short T2 tissues. Magn Reson Med 2021; 86(2):881-892.
20. Dimov A V., Liu Z, Spincemaille P, Prince MR, Du J, Wang Y. Bone quantitative susceptibility mapping using a chemical species-specific R_2^* signal model with ultrashort and conventional echo data. Magn Reson Med 2018; 7(1):121-128.
21. Jang H, Drygalski A, Wong J, et al. Ultrashort echo time quantitative susceptibility mapping (UTE-QSM) for detection of hemosiderin deposition in hemophilic arthropathy: a feasibility study. Magn Reson Med 2020; 84(6):3246-3255.
22. de Mello R, Ma Y, Ji Y, Du J, Chang EY. Quantitative MRI musculoskeletal techniques: an update. AJR Am J Roentgenol 2019; 213(3):524-533.
23. Ronneberger O, Fischer P, Brox T. U-net: Convolutional networks for biomedical image segmentation, MICCAI 2015: 18th international conference, Munich, Germany, October 5-9, 2015, proceedings, part III 18. Springer International Publishing, 2015: 234-241.
24. Hesamian MH, Jia W, He X, et al. Deep learning techniques for medical image segmentation: achievements and challenges. J Digit Imaging 2019; 32:582-596.
25. Liu F, Feng L, Kijowski R. MANTIS: model-augmented neural network with incoherent k-space sampling for efficient MR parameter mapping. Magn Reson Med 2019; 82:174-188.
26. Liu F, Zhou Z, Jang H, Samsonov A, Zhao G, Kijowski R. Deep convolutional neural network and 3D deformable approach for tissue segmentation in musculoskeletal magnetic resonance imaging. Magn Reson Med 2018; 79(4):2379-2391.
27. Yoon J, Gong E, Chatnuntawech I, Bilgic B, Lee J, Jung W, Ko J, Jung H, Setsompop K, Zaharchuk G, Kim EY, Pauly J, Lee J. Quantitative susceptibility mapping using deep neural network: QSMnet. Neuroimage 2018; 179:199-206.
28. Zhao Y, Wang X, Che T, Bao G, Li S. Multi-task deep learning for medical image computing and analysis: A review. Comput Biol Med 2023; 153:106496.
29. Liu W, Liu X, Li H, Li M, Zhao X, Zhu Z. Integrating lung parenchyma segmentation and nodule detection with deep multi-task learning. IEEE J Biomed Health Inform 2021; 25:3073–3081.
30. Wang X, Jiang L, Li L, Xu M, DengX, Dai L, Xu X, Li T, Guo Y, Wang Z, Dragotti PL. Joint learning of 3D lesion segmentation and classification for explainable COVID-19 diagnosis. IEEE Trans Med Imaging 2021; 40:2463–2476.
31. Cao L, Li L, Zheng J, Fan X, Yin F, Shen H, Zhang J. Multi-task neural networks for joint hippocampus segmentation and clinical score regression. Multimed Tools Appl 2018; 77:29669-29686.
32. Sui B, Lv J, Tong X, Li Y, Wang C. Simultaneous image reconstruction and lesion segmentation in accelerated MRI using multitasking learning. Med Phys 2021; 48:7189-7198.
33. Lim, H. Transformer-Based Integrated Framework for Joint Reconstruction and Segmentation in Accelerated Knee MRI. Electronics 2023; 12:4434.
34. Kohn MD, Sassoon AA, Fernando ND. Classifications in brief: Kellgren-Lawrence classification of osteoarthritis. Clin Orthop Relat Res 2016; 474(8):1886-1893.
35. Klein S, Staring M, Murphy K, Viergever MA, Pluim JPW. Elastix: a toolbox for intensity-based medical image registration. IEEE Trans Med Imaging 2010; 29:196-205.

36. Wu M, Zhao W, Wan L, et al. Quantitative three-dimensional ultrashort echo time cones imaging of the knee joint with motion correction. NMR Biomed 2020; 33:e4214.
37. Virtanen P, Gommers R, Oliphant TE, et al. SciPy 1.0: fundamental algorithms for scientific computing in Python. Nat Methods 2020; 17:261-272.
38. Abramson RG, Su PF, Shyr Y. Quantitative metrics in clinical radiology reporting: a snapshot perspective from a single mixed academic-community practice. Magn Reson Imaging 2012; 30:1357-1366.
39. Vikas Gulani, and Nicole Seiberlich. Quantitative MRI: Rationale and Challenges. Elsevier, 2020, https://doi.org/10.1016/B978-0-12-817057-1.00001-9.
40. Xue Z, Xin B, Wang D, et al. Radiomics-enhanced multi-task neural network for non-invasive glioma subtyping and segmentation, International Workshop on Radiomics and Radiogenomics in Neuro-oncology. Cham: Springer International Publishing, 2019: 81-90.
41. Wang X, Jiang L, Li L, et al. Joint learning of 3D lesion segmentation and classification for explainable COVID-19 diagnosis. IEEE Trans Med Imaging 2021; 40(9):2463-2476.
42. Zhou X, Qiu S, Joshi PS, et al. Enhancing magnetic resonance imaging-driven Alzheimer's disease classification performance using generative adversarial learning. Alzheimers Res Ther 2021; 13(1):60.
43. Yang G, Yu S, Dong H, et al. DAGAN: Deep dealiasing generative adversarial networks for fast compressed sensing MRI reconstruction. IEEE Trans Med Imaging 2018; 37:1310-1321.
44. de Moura HL, Menon RG, Zibetti MVW, Regatte RR. Optimization of spin-lock times for $T_{1\rho}$ mapping of human knee cartilage with bi- and stretched-exponential models. Sci Rep 2022; 12(1):16829.